Kinetic pathways of sheared block copolymer systems derived from Minkowski functionals

G. J. A. Sevink, and A. V. Zvelindovsky

Citation: The Journal of Chemical Physics **121**, 3864 (2004); doi: 10.1063/1.1774982

View online: https://doi.org/10.1063/1.1774982

View Table of Contents: http://aip.scitation.org/toc/jcp/121/8

Published by the American Institute of Physics

Kinetic pathways of sheared block copolymer systems derived from Minkowski functionals

G. J. A. Sevink and A. V. Zvelindovsky
LIC, Leiden University, P.O. Box 9502, 2300 RA, Leiden, The Netherlands

(Received 23 March 2004; accepted 27 May 2004)

We employ Minkowski functionals to analyze the kinetics of pattern formation under an applied external shear flow. The considered pattern formation model describes the dynamics of phase separating block copolymer systems. For our purpose, we have chosen two block copolymer systems (a melt and a solution) that exhibit a hexagonal cylindrical morphology as an equilibrium structure. Our main objective is the determination of efficient choices for the treshold values that are required for the calculation of the Minkowski functionals. We find that a minimal set of two treshold values (one from which should be equal to an average density value and another to a higher density value) is sufficient to unraffle the phase separation kinetics. Given these choices, we focus on the influence of the degree of phase separation, and the instance at which the shear is applied, on the kinetic pathways. We also found a remarkable similarity of the time evolution of Euler characteristic and the segregation parameter for the average density choice. © *2004 American Institute of Physics.* [DOI: 10.1063/1.1774982]

I. INTRODUCTION

Many phenomena in nature produce complex spatio-temporal patterns. Although the interactions due to which these patterns are formed can be simple, the dynamics of patterns can be quite nontrivial. Examples of such systems are cellular automata, superconductors of first and second type, Rayleigh-Bernard cells in liquids, Belousov-Zhabotinski chemical reactions, and block copolymers. Block copolymers are long, often flexible, molecules consisting of chemically different blocks. In a melt or solution they tend to microphase separate (bringing similar blocks together) under certain conditions, on a scale that is set by the blocks characteristic length, often nanometers.[1] Microphase separation leads to the formation of periodic structures similar to crystals. However, upon formation, the patterns are often highly defected and far from perfect. As block copolymers are fluids with high overall viscosity, the resulting characteristic times for defect movement and annihilation can be very long. Moreover, processing conditions such as shear[2,3] or applied electric fields can influence this behavior and determine to a large extend how the phase separation can proceed. Determining the symmetry groups for a defected structure is often a difficult task both experimentally and theoretically. In computer simulations one obtains information on the three-dimensional microstructure. As the structure is often very defected, simple visual inspection is not sufficient. Fourier analysis is a common procedure in this case, but helps only if structure is already mostly periodic. In the initial stages of microphase separation the structure is often reminiscent to the periodic one, but deformed—stretched, squeezed, etc. This is in particular the case if the system is subjected to external fields such as for instance shear flow. In this situation the analysis of topological and geometrical quantities, followed by an expression for the similarity measure with respect to perfect structures, would be of great help. The efficient tool for this are additive image functionals like Minkowski functionals. Minkowski functionals were proven to be very valuable for the description of complex morphologies in many areas of science, ranging from phase separating (block co)polymer systems[4–11] like the one considered here, complex fluids,[12–15] composite materials,[14] reaction-diffusion systems,[15,16] to large-scale structures in the universe.[15,17,18] An extensive review, including many examples of application, was recently published.[19] This field is still growing; a new and very promising vectorial Minkowski functional was recently developed by Klaus Mecke.

In many cases the structures are given by fields on a grid: density fields or order parameter fields. In the procedure for the calculation of the Minkowski functionals, there is a question of choosing the so-called threshold value for images. For fields, this choice is basically equal to the choice of the position of interfaces in a microstructure. Usually one presents Minkowski functionals for a set of several threshold values. As the values of the Minkowski functionals are sensitive to these values, the interpretation of results is not unique. Here we demonstrate that the threshold value can be chosen based upon physical considerations. We show that this choice is crucial for the correct interpretation of a dynamical pathway of a pattern.

II. PATTERN FORMATION IN BLOCK COPOLYMER SYSTEMS

We give a short outline of the theory used in the simulations; for more details see Refs. 20, 21 and references therein. We model the pattern formation that occurs when a block copolymer melt or solution is brought into a state where the chemically different blocks phase separate on a mesoscopic level (1–1000 nm). In our model, a block copolymer molecule is represented by a Gaussian chain, con-

sisting of N beads. Each bead typically represents a number of chemical monomers. Differences in monomers gives rise to different bead species (for example, $A_{N_A}B_{N_B}$, for a diblock copolymer, $A_{N_A/2}B_{N_B}A_{N_A/2}$, for a symmetric ABA-triblock copolymer; $N=N_A+N_B$). The three-dimensional volume of the simulated system is denoted by V^{syst}, and contains n Gaussian chains. Solvents are incorporated as single beads.[22] The interchain interactions are incorporated via a mean field with interaction strength controlled by the Flory-Huggins parameters χ_{IJ}. The microstructure patterns are described by the coarse grained variables, which are the density fields $\rho_I(\mathbf{r})$ of the different species I. Given these density fields a free energy functional $F[\rho]$ can be defined as follows:[20–22]

$$F[\rho]=-kT\ln\frac{\Psi^n}{n!}-\sum_I\int_{V^{\mathrm{syst}}}U_I(r)\rho_I(r)dr+F^{\mathrm{nid}}[\rho]. \quad (1)$$

Here Ψ is the partition function for the ideal Gaussian chain in the external fields U_I and F^{nid} is the contribution due to the nonideal mean-field interactions. The external potentials U_I and the density fields ρ_I are bijectively related in a self-consistent way via a density functional for Gaussian chains. Several methods can be employed to find the minimum of free energy [see Eq. (1)] and equilibrium density fields $\rho_I(\mathbf{r})$. They can roughly be divided into *static* and *dynamic* methods, although a number of hybrids exist which are generally referred to as quasidynamic methods (for instance[23]). A rather complete and recent review is given in Ref. 24. In this article, we use a dynamic scheme that has been developed within our group. An advantage of this scheme is that it intrinsically considers dynamic pathways towards a free energy minimum, including visits to long-living metastable states. In this sense, the model can be seen to mimic the experimental reality when compared to static schemes, which are optimizations, based upon mathematical arguments. The thermodynamic forces driving the pattern formation in time are the gradients of the chemical potential $\mu_I(r)=\delta F/\delta\rho_I$[20–22]

$$\frac{\partial\rho_I}{\partial t}=M_I\nabla\cdot\rho_I\nabla\mu_I+\eta_I, \quad (2)$$

where M_I is a constant mobility for bead I and $\eta_I(\mathbf{r})$ is a noise field, distributed according to the fluctuation-dissipation theorem. In the presence of a steady shear flow, with velocity $v_x=\dot{\gamma}y$, $v_y=v_z=0$, an extra convection term is added to the right-hand side of the diffusion equation (2) equal to $-\dot{\gamma}y\nabla_x\rho_I$. Here $\dot{\gamma}$ is the shear rate (the time derivative of the shear strain γ) and sheared boundary conditions apply.[20,25–28]

III. MINKOWSKI FUNCTIONALS

Determining the underlying fundamental mechanisms in the structure transformation in block copolymers is a difficult task. The huge scales in space and time covered by our (parallel implemented) simulation technique, hampers us from grasping the important features from imaging the four-dimensional (4D) data alone. To give an idea: for each of the simulations considered in this article, the amount of data is as large as $64\times64\times64=262\,144$ double-precision (8 bytes) spatial data times 600 (writing spatial information every 50 time steps for a total of 30 000 time steps), resulting in a total amount of data for each simulation of almost 1.3 Gbyte. Modern integral-geometry morphological image analysis provides the tool to assign numbers to the shape and connectivity of patterns formed by pixels of 3D images, by means of additive image functionals. An example of such additive image functionals are the Minkowski functionals, that describe the morphological information contained in an image by numbers that are proportional to very simple geometrical and topological quantities: the volume V, the surface area S, the mean curvature H, and the Euler characteristic χ. The first step in the analysis of the information contained in our density fields is therefore to compute the Minkowski functionals themselves. This is not a direct procedure: a thresholding step must be performed to generate a black-and-white image from the density fields, prior to the Minkowski functional calculation. A complicating factor, that will be considered in detail in the remainder, is the resulting dependency of the Minkowski functional values on the choice of the threshold. The second step is to study the behavior of the four numbers as a function of time.

A. The calculation procedure

The implementation of the numerical calculation of the Minkowski functionals used here, is adapted from the work of Michielsen and de Readt.[19,29] A short overview is presented here for completeness. The starting point is a 3D density field ρ, that is the output of our simulations at a time step (TMS). Our calculations are carried out on a grid (although this grid is only introduced in the implementation of the continuous equations). The picture $\mathcal{P}$ that is described by the Minkowski functionals, is build up from the reference field $\rho(\mathbf{r})$ in the following way:

$$\mathcal{P}(\mathbf{r})=\Theta(\rho(\mathbf{r})-h), \quad (3)$$

where $\Theta(x)$ is the Heaviside step function, giving 1 or 0. In other words, the black-and-white picture $\mathcal{P}$ (with black pixels representing the object, and white pixels the background) is build up from the field ρ by thresholding, and setting the values of the thresholded field to binary valued pixels. One should keep in mind that the resulting picture $\mathcal{P}$ (and its corresponding Minkowski functional values) is also a function of the choice of the threshold value h: $\mathcal{P}(\mathbf{r})$ is in fact $\mathcal{P}(\mathbf{r},h)$. The picture $\mathcal{P}(\mathbf{r},h)$ can be completely described in terms of Minkowski functionals.

We consider each pixel as a union of the disjoint collection of open elements of length Δx (with Δx the discretization length): n_c interiors, n_f faces, n_e edges, and n_v vertices. For a single cubic 3D pixel, the number of these basic elements are: $n_c=1$, $n_f=6$, $n_e=12$, and $n_v=8$. The procedure that follows is simple due to the additivity: the values for the complete image $\mathcal{P}$ are calculated by simply adding black pixels to an initially completely white background (where all geometrical and topological values are equal to zero). The pixels themselves are build from the disjunct elements, for which the Minkowski functional values (or similarly, its

morphological and geometrical counterparts) can easily be calculated.[19] This leads to a very simple expression for the geometrical and topological quantities of a three dimensional object,

$$V=n_c, \quad S=-6n_c+2n_f, \quad 2H=3n_c-2n_f+n_e,$$
$$\chi=-n_c+n_f-n_e+n_v. \tag{4}$$

The implementation is therefore very straightforward (it can be found in Ref. 29), and should only be optimized with respect to double counting. As our simulations are carried out with periodic boundary conditions, we update boundaries prior to the Minkowski functional calculation by a common procedure: we add an extra layer at all sides of the original grid with the correct (periodic) boundary values. As the procedure described above is based on the information that is contained by the grid, we also compared the results of our calculation with a method that interpolate the grid values by a marching cube algorithm.[30] Especially the surface area S and mean curvature H may deviate between the two, due to the rather crude discretization used in our method. However, for the box size under consideration, we found that this discretization effect is negligible.

B. Relation between structure topology and Euler characteristics

The Minkowski functional χ of Eq. (4) is the same as the Euler characteristic defined in algebraic topology. Using this equality, the Minkowski functional χ can be understood as the number of connected components minus the number of tunnels (holes) plus the number of cavities. For instance, $\chi=1$ for a solid sphere, $\chi=2$ for a hollow sphere, $\chi=0$ for a torus, and $\chi=-1$ for ∞ shape which has two holes. Due to the additivity, we can use this knowledge for the determination of the topology of the majority part of the local structures from the Euler characteristic. For AB and ABA block copolymers, the amount of amenable mesostructures is limited to micellar, cylindrical, bicontinuous, or lamellar morphologies. This observation leads to a few very simple rules for the interpretation of structures: very positive χ can be interpreted as majority of micellar (spherical or cylindrical) structures, very negative χ as highly connected structures with many tunnels. From the Euler characteristic it is impossible to distinguish between spherical and cylindrical micelles; we therefore will refer to these structures as micelles. An Euler characteristic $\chi=0$ can be interpreted as a collection of tori, which, due to the periodic boundary conditions, is equal to a collection of highly oriented cylindrical domains.

C. The choice of the threshold

A normal procedure is to split the interval of amenable density values on the grid (in our case [0,1]) into 256 bins of equal width; the number 256 reflects the number of levels that are present in a 8 bits greyscale image. Consequently, a threshold value $h^{bin}\in\{0,..,255\}$ is chosen, and the picture $\mathcal{P}$ is constructed by placing black pixels (of binary value 1) using Eq. (3), with $h=h^{bin}/255$. Considering all 256 threshold values as a function of time would lead to high redundancy and an explosion of data that is difficult to interpret. A standard approach is to choose one value of the threshold; often this value is taken $h^{bin}=128$ ($h\approx 0.5$). In the remainder, we show how to use physical knowledge about our system to condition the choice of the threshold, and therefore limit the amount of data generated.

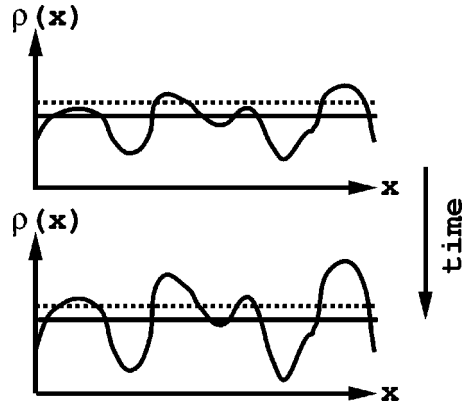

FIG. 1. Schematic view on the influence of the threshold choice in 1D case. From top to bottom: development of density inhomogeneity $\rho(x)$ (nonmonotonic line) as a function of spatial coordinate x in course of time due to the progress of phase separation. Straight solid line—level of average density; dashed line—an arbitrary level.

All calculations [we numerically solve Eq. (2)] start from uniform density fields $\rho_I(\mathbf{r})=\rho_I^0$, with ρ_I^0 the average density or average concentration of block I. This reflects the case were all components are completely mixed. During the simulation, the total concentration of all species I remains constant. Let us consider a system in course of time. The first step of simulation corresponds to a quench of the system into an ordered phase. Locally, deviations of the average value ρ_I^0 start to develop, in time leading to a final fully phase-separated melt or solution with values $\rho_I(\mathbf{r})$ between the natural extremes 0 and 1. The starting and final states of the system both have distinct different features. A schematic illustration can be found in Fig. 1. Phase separation consists of two simultaneous processes: the amplitude of the deviation of the density from its average value grows in time, and domains of density inhomogeneity change their shape and size. Let us consider the first process. In Fig. 1 we sketch the growth of density inhomogeneity for a 1D system. If we choose the threshhold value equal to the average density (solid straight line), the picture $\mathcal{P}$ will have the same features (connectivity, domain size) for the upper and lower sketches. For an arbitrary threshold value (dashed line) the features will be very different: the lines cross the graphs in different positions, therefore both the connectivity and domain shape (and even the number of domains) will be different. In this case, the picture $\mathcal{P}$ is a view on ''the top of the iceberg.'' For the second process, where the domains change as well, the top of the iceberg view is very sensitive to small changes in inhomogeneity. Changes in domain shape and connectivity will be in particular seen under the influence of externally applied shear flow. Therefore by combining two threshold choices, from which one is equal to the average density value ($h=\rho^0$), one can separate information originating from the two processes that contribute to phase separation.

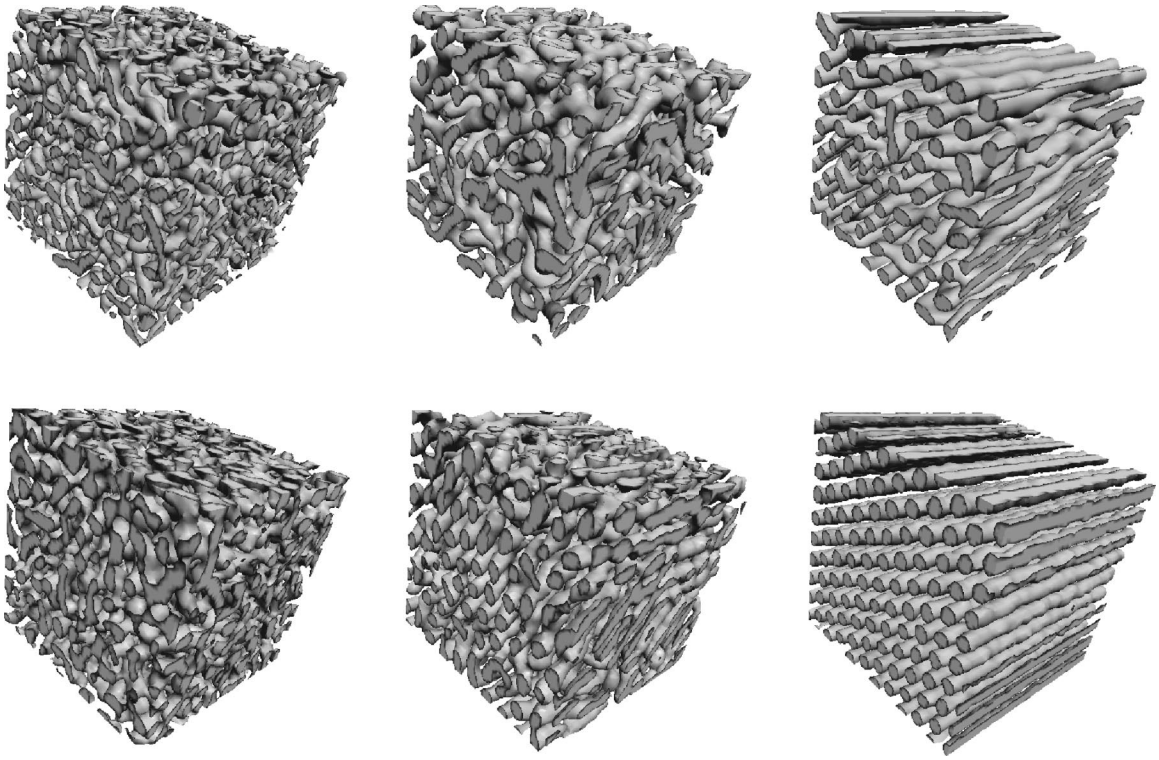

FIG. 2. Top: snapshots of the A_3B_7 diblock copolymer melt. Bottom: snapshots of the 55% solution of $A_3B_9A_3$ triblock copolymer in a one-bead solvent. The block interaction parameters for the solution were previously published in van Vlimmeren *et al.* (Ref. 22), for the melt $\epsilon_{AB}=7.5$ kJ/mol. The shear parameter was chosen $\tilde{\gamma}=0.001$ [see (Ref. 20) for details]. The snapshots are taken at dimensionless time steps (from left to right): 200, 2000, and 25 000 TMS. Fot the both systems, shear was applied from TMS=0. The snapshots show isosurfaces of the cylinder forming component at $\rho_I=0.33$.

In the applications we will therefore consider two choices for the systems under consideration: $h=0.5$ and $h=\rho^0$.

IV. APPLICATION

We analyze the dynamics of structure formation of two block copolymer systems under an applied shear flow. One system is a diblock copolymer melt, the other is a solution of triblock copolymer. The chain architecture and presence of the solvent might have an influence on the kinetics. Although the systems differ in several respects, they both form a cylindrical microstructure, which in equilibrium would be a perfect array of hexagonally packed cylinders. In absence of the applied shear, the cylinders would be hexagonally packed on a local scale, but the orientation on a larger scale would be isotropic, and the structure would have many defects of relatively low energy.[22] We study two shear scenarios, which differ in the moment that shear was applied to the systems. This allows us to clarify the influence of shear on both processes occurring during phase separation: the growth of density inhomogeneity and change of domains. The evolution of both structures in the first shear scenario is shown in Fig. 2. Shearing of the second system in the second shear scenario was previously published in Ref. 31. Visual inspection of images confirms the development of hexagonally arranged cylinders from an initially poor structure. Initial stages (first two images in each row) do not exhibit easily spotted differences, while the more developed structure is clearly more defected in case of a melt. Two mechanisms play a role in the formation of a structure: microphase separation is dominant at the initial stages, orientation of domains is predominant at later stages. To deduct the details of the processes and their interplay, one needs to examine a tremendous number of images in three dimensions. Some guiding is obviously very desirable. Fourier transformation gives some information on later stages of alignment process, but is not conclusive at the initial stages.[31] Although visual inspection suggests that there is a difference in the development of well aligned cylinders between the melt and the solution, no decisive conclusion is possible.

We can characterize the degree of phase separation in a system by considering a segregation parameter $P_I=\overline{\rho_I^2}-(\rho_I^0)^2$ (we omit the index I in the remainder as we will always consider the cylinder forming component).[22] In a homogeneous system $P=0$, while in totally segregated systems $P^{\max}=\rho^0-(\rho^0)^2$ (provided that the sum density of all components is chosen to be 1). For the melt system under consideration $\rho^0=0.3$, while for the solution $\rho^0=0.33$, which gives roughly the same $P^{\max}$ in both cases. Figure 3 shows the time evolution of the segregation parameter for the two systems. The segregation parameter for the triblock copolymer solution is an order of magnitude lower than for the diblock copolymer melt. The reason for this difference is that for the considered Flory-Huggins interaction parameters the degree of segregation is higher for the melt than for the solution. This clarifies our choice of systems: we can study the kinetics of phase separation in systems having very different degrees of phase separation but the same equilibrium micro-

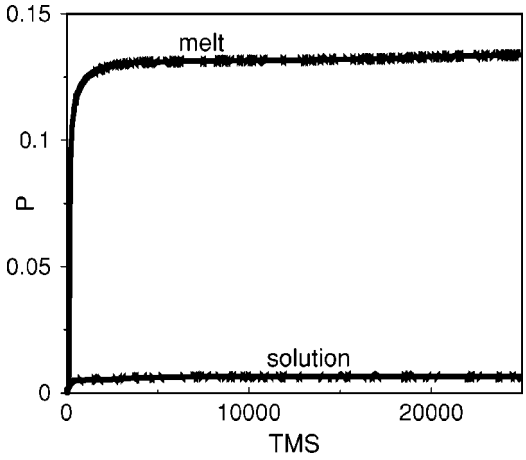

FIG. 3. The segregation parameter P as a function of time for the cylinder forming component. Shear is applied from TMS=0. The noisiness of the lines is a reflection of the noise in the dynamic equations.

structure (cylinders), and, moreover, roughly the same average density of the cylinder forming block. If we would choose one polymeric composition, say a diblock copolymer melt, and vary the degree of phase separation by varying the Flory-Huggins parameters to have to same large difference in separation, we would necessarily shift into the phase space where system experiences another symmetry, different from cylinders.

As one could expect from a global parameter such as P, it monitors the degree of phase separation rather well, but does not give any information on local rearrangements in the structure. To this aim, we consider the Minkowski functionals as a function of time, that were calculated by the expression of equation Eq. (4). Following the motivation discussed in the preceding section we consider two different choices of threshold value: $h=\rho^0$ and an arbitrary one, $h=0.5$.

The Euler characteristic is most illustrative. For the solution (Fig. 4, top) we observe a large influence of the choice of the threshold: choice $h=\rho^0$ shows a very positive Euler characteristic, while for $h=0.5$ this number is very negative. For both choices, the limiting behavior of the Euler characteristic with increasing time is zero, which is reached at the same instance in time. This value can be associated with the state of well aligned cylinders (see Sec. III B), as we can also see from Fig. 2. The fact that the Euler characteristics at later stages coincide is therefore expected, as the equilibrium morphology of aligned cylinders is reached at an early stage (around TMS=10 000) and the degree of phase separation and the position of the interfaces in space does no longer significantly change. The Euler characteristic for the melt (Fig. 4, bottom) is distinctively less sensitive to the different choices of the threshold. For both choices, the Euler characteristic is negative at the initial stages, be it that the Euler characteristic is significantly lower for $h=0.5$. At later stages, the two curves approach and coincide to the end. Based on the Euler charateristic, the two polymer systems would have completely different kinetic pathways of phase separation depending on the choice of the threshold. However, the difference is not so surprising as it might look at the first glance. If the threshold is chosen at average density

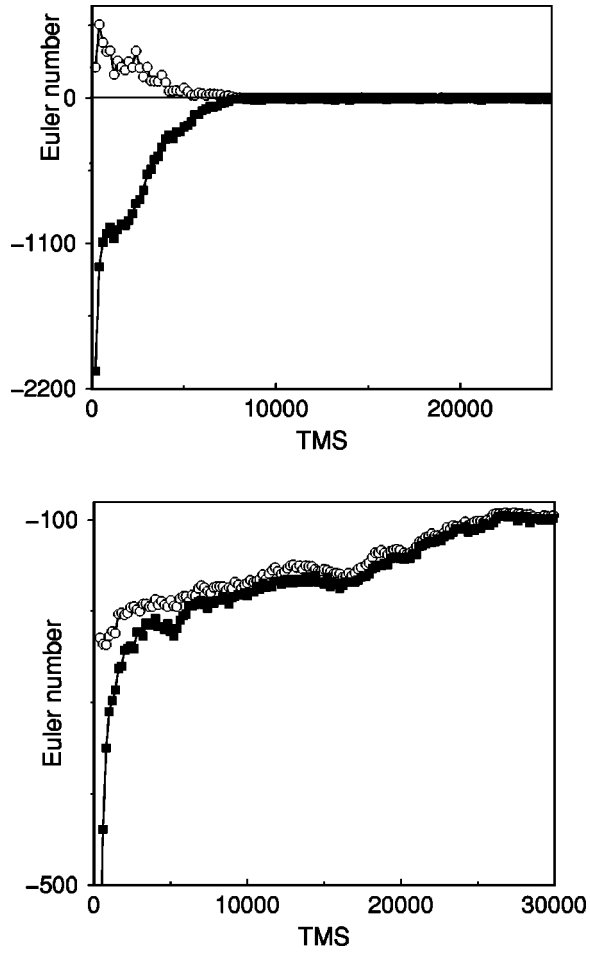

FIG. 4. The Euler characteristic as a function of time for the cylinder forming component in the solution (top) and in the melt (bottom). The shear was applied starting from TMS=0. The Euler characteristics were calculated for two choices of the threshold parameter: $h=\rho^0$ (○), and an arbitrary one, $h=0.5$ (■).

value (■ in the graphs) both systems develop themselves starting from the initially highly interconnected network (very negative Euler number) towards infinite cylinders (tori), slowly reducing the number of connections and therefore holes. This threshold value ''sees'' all density deviations around ρ^0, even very small ones. As it is clear from the sketch in the Fig. 1 the topological picture of higher density modes will be different. If the arbitrary value h is higher then ρ^0 (as in our case), less interconnections will be seen, as they have lower density values then tops of the iceberg. Due to that reason the Euler number for both systems is higher in case of $h=0.5$ (○ in the graphs). Moreover, if the system has a lower degree of phase separation (as the solution in our case, Fig. 3) the number of ''seen'' interconnections is even less. In this case, the density deviations overshooting the $h=0.5$ value will be mostly seen as topological micelles, and the Euler number will be positive (Fig. 4, top, ○). As the micelles grow and merge into the cylinders (tori), the Euler number levels down. As a result, by combining information from the evolution of the Euler characteristic for two choices, we conclude that there are two simultaneous processes in the kinetic pathway of the structure rearrangement in a flow. One is removement of interconnections (defects)

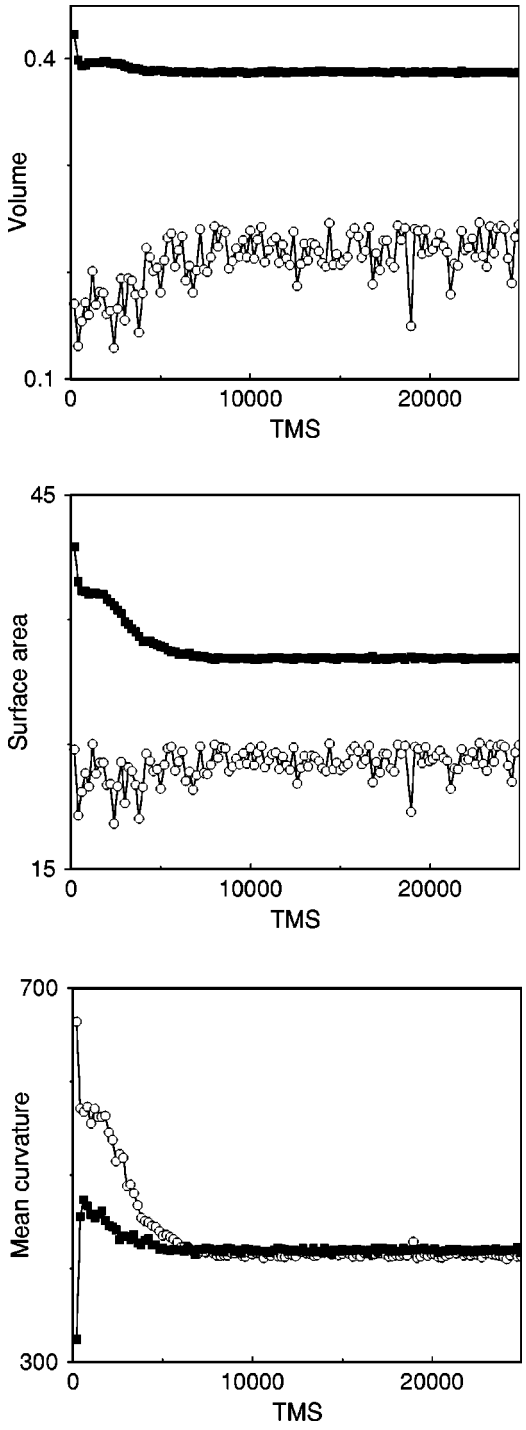

FIG. 5. The volume, surface area, and mean curvature as a function of time of the cylinder forming component for the solution. The shear was applied starting from TMS=0. The Minkowski functionals were calculated for two choices of the threshold parameter: $h=\rho^0$ (○), and an arbitrary one, $h=0.5$ (■).

between cylinders and another is merging of micelles into cylinders. The relative contribution of these processes into the pathway depends on the degree of phase separation.

Figure 5 shows the volume, surface area, and mean curvature for one of the polymer systems (the solution) for the two different choices of the threshold. The volume and surface area for $h=0.5$ are lower than for $h=\rho^0$ simply due to the fact that there are always less regions with high densities than with the average one. The fact that the volume and surface area are noisy for $h=0.5$ shows that the high-density field values are much more sensitive to the breakage and reformation of local structures. Partial melting of already phase separated structures makes them drop out of the thresholded image. Then they emerge again, first as micelles. As the number of structures with high-density values is lower, the noisiness in graphs is higher. The volume for $h=\rho^0$ decreases fast in the very beginning of the phase separation and then stays constant. The most drastic drop in volume corresponds to the times when phase separation shoots up (see Fig. 3). At that stage the system microphase separates from the initially homogeneous state, decreasing the contacts between different blocks and therefore lowering the enthalpic contribution to the free energy. The slight increase of the volume for $h=0.5$, however, is much slower. It corresponds to the fact that high-density regions are still growing while phase separation continues, as it is seen on slight increase of segregation parameter P on the same time scale (Fig. 3). As the volume value in this case is smaller than for $h=\rho^0$ this increase does not contradicts with the decrease of the total free energy. The surface area for $h=\rho^0$ is decreasing, which suggests that the surface tension of such an interface is positive. As the surface area levels out at the same time as the Euler characteristic, this suggests that the main mechanism of reducing surface area is due to removal of interconnections in the structure. The surface area of high-density domains ($h=0.5$) is roughly constant (after averaging over the noise). The volume in this case is slightly increasing, suggesting that the domains adapt a more round shape in the cross section; a mechanism that indeed occurs with cylinders in a flow, see Fig. 2. The mean curvature for both threshold choices decreases (apart from the very first stages of phase separation for the choice $h=\rho^0$). The monotonic decrease after the initial stages suggests positive bending constants of the interfaces. The two graphs of the mean curvature are qualitatively very different in the very first stages of phase separation (see Fig. 3 as well). At that stage the interfaces are only developing. The mean curvature for the average density choice $h=\rho^0$ rapidly grows at the very beginning. In this case the system starts to develop from the homogeneous density ρ^0, and initially consists of a network of interconnections with very diffuse interfaces, induced by the noise. This network of interconnections is rich of saddle points which have low mean curvature. While phase segregation progresses and the network of interconnections coarsens, the interconnections become longer and posses substantial cylindrical parts in between. As a result, the mean curvature increases. As the interface develops, the process continues mostly by breaking interconnections (therefore reducing the number of saddle regions), and the mean curvature drops. For the high-density domains ($h=0.5$) the decrease is persistent during the evolution and is much more drastic due to the fact that the system for this threshold choice consists initially of spherical micelles with have higher curvature than that of final cylindrical micelles. In this case the interface is only seen starting from $h=0.5>\rho^0$ and therefore will be simply absent during first few time steps. This is not

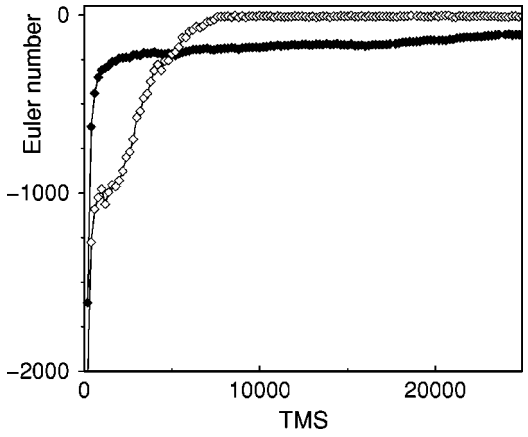

FIG. 6. The Euler characteristic as a function of time of the cylinder forming component for two systems. The melt is denoted by ♦, the solution by ◇. Shear was applied at TMS=0.

observed in the graph, because the system is first stored after 50 time steps.

In the remainder, we will concentrate on the Euler characteristic as a function of time. We have seen already, that the Euler characteristic is a valuable means to distinguish the dominant mechanisms in kinetic pathways. If we compare the melt and the solution (Fig. 6) for the threshold $h=\rho^0$, we see that the topological pathways are distinctly different. In the melt, initially there are less connections than in the solution, and most of the connections are easily removed. The remaining connections are very long living. The growth of the Euler number for the solution is initially slower, and has a small characteristic plateau around the first thousands time steps. After this temporarily stagnation, the Euler number continues to grow, overshoots the values for the melt, and reaches the state of perfect cylinders, much more perfect than the melt system (compare also final images in Fig. 2). This difference can be explained bearing in mind the results for the second choice of the threshold value, Fig. 4. The solution is a much less segregated system than the melt (see Fig. 3). High-density regions appear as micelles in the first stages of phase separation (Fig. 4, top, ○). The micelles will be seen also at lower threshold values, in reduced quantity, among newly emerging structures. In the very beginning the number of micelles grows (increase in Fig. 4, top: ○). The same process may be expected at other threshold values. This, together with breakage of interconnections, contribute to the initial fast growth of Euler number at $h=\rho^0$. Consequently, the number of micelles is decreasing, as they merge into the cylinders. For $h=\rho^0$ the two processes (a decrease of micelles and breakage of interconnections) therefore balance each other, resulting in a short plateau in the Euler number graph. Finally, when most of the micelles have disappeared, the second processes takes over and the system proceeds towards a perfect cylindrical phase. One should bear in mind that as the solution is much less segregated than the melt, new micelles will appear and coalesce all the time, which is making the initial slope of the curve smaller than the one for the melt system.

As we have two processes in the phase separation involved, namely, development of interfaces and domain rearrangement, one should study to what extend shear affects either of them. In the preceding paragraphs we discussed the case of shear applied from the start. Here, we proceed with a discussion of the case where the shear was applied well after the interfaces were formed, so that we can separate the two processes. The significance of the instance at which the shear is applied can already be seen in the segregation parameter, as shown in Fig. 7. For both systems we have studied two cases: case 1 where the shear is applied from the beginning, and case 2 where the shear is applied to an already phase separated structure at a later instance. The influence of shear is stronger for a weaker separated system (solution, Fig. 7, top). In both melt (see inset in Fig. 7, bottom) and solution we see the enhancement of phase separation by shear at the very first stage, when the interfaces are formed. After the first thousand time steps the shear starts to suppresses the phase separation in both systems. That could be due to the fact that, at this stage, the domain rearrangement starts to play a major

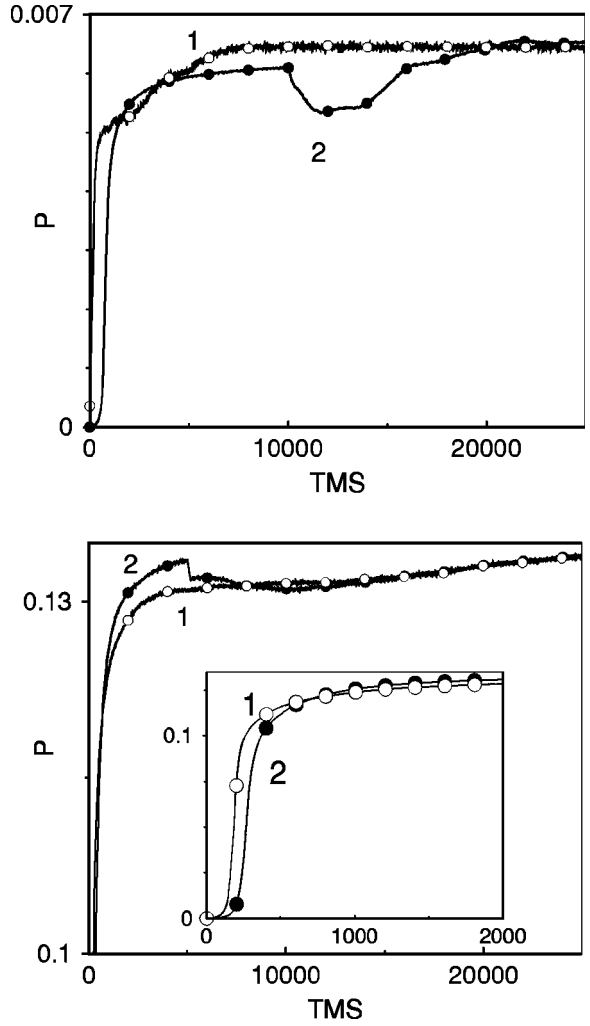

FIG. 7. The segregation parameter P as a function of time of the cylinder forming component for the solution (top) and the melt (bottom) at different shear scenarios. The label 1 (○) refers to the situation where the shear is applied from the beginning; label 2 (●) refers to the case where the shear is applied at TMS=5000 (melt) and TMS=10 000 (solution). The inset in the bottom figure focusses on the enhancement of phase separation by shear at the very early stages in the melt system. The noisiness of the lines is a reflection of the noise in the dynamic equations.

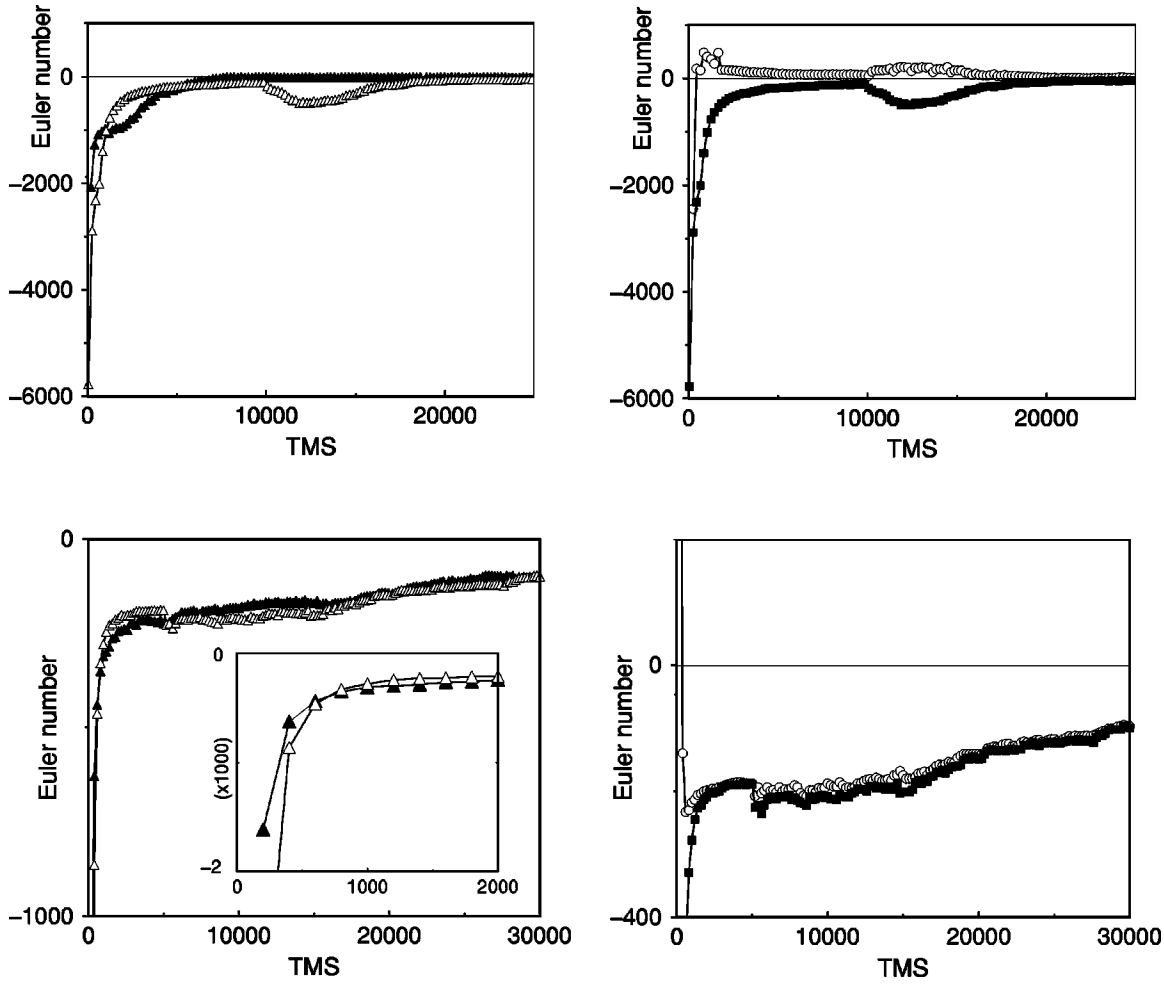

FIG. 8. Euler characteristics as a function of time of the cylinder forming component for the solution (top) and melt (bottom). Left: $h=\rho^0$; the shear initiated from the beginning (▲) and at later instance (△), which is TMS=10 000 for the solution and TMS=5000 for the melt. The inset in the bottom figure focusses on the very early stages of the Euler characteristic for the melt system. Right: $h=\rho^0$ (○), and $h=0.5$ (■); the shear initiated at TMS=10 000 for the solution and TMS=5000 for the melt.

role. The shear breaks some domains such that they can reconnect in the flow direction.[27,31] This phenomena is equivalent to partial melting of the microstructure, and the segregation parameter is therefore lower. This region is, however, relatively short for the solution when compared to the melt (for the melt this region extends until the instance where shear is applied in case 2, TMS=5000). This could be explained by the fact that, as the solution is a much weaker segregated system than the melt, the domain breakage by shear occurs easier in the solution. By the time most of the interconnections are removed, the system consists of cylinders in the direction of flow. In general, the system without interconnections is in true equilibrium (without shear), and has a lower free energy than the system with interconnections. Therefore, if the system reaches that state of perfect cylinders in the flow direction, it continues to enhance the interfaces, and has a higher segregation parameter than the system without shear, full of structural defects like interconnections. The much stronger segregated melt system did not reach the perfect cylinder state even after longer shear, so it is simply not yet in the state just discussed for the solution. The kinetics of defect removal in the stronger segregated system is simply slower. When shear is applied at a later instance, to an already well separated system, partial melting occurs (drop in P in Fig. 7). The weaker the phase separation in the system the more the structure melts. This melting consists of two contributions, one of which is due to overall partial melting of the interfaces, and second and most profound is due to the breakage of domains like interconnections and cylinders. Both systems recover and reach the same segregation parameter value as in the scenario where the shear was applied form the beginning. Therefore, both systems do not have a long memory of the shear history.

The Euler number gives more information of the kinetic pathways for the above mentioned shear scenarios. We further elaborate on the effect of different shear instances and threshold choices in Fig. 8. In this figure, the left column shows the Euler characteristics for choice $h=\rho^0$ of the threshold and different instances of applied shear; the right column shows the effect of difference choices of the threshold for the second shear scenario (where the shear was applied at a later instance). The Euler graphs in the left column of Fig. 8 are remarkably similar to the graphs of the segregation parameter P for the same systems (shown in Fig. 7). All conclusions which have been just drawn on basis of the segregation parameter P in Fig. 7 and previous knowledge

derived from the visual inspection of many 3D images[31] can be also made solely on the basis of Euler number graphs in Fig. 8 (left). Moreover, the information contained by the graphs of the Euler characteristic is much richer. The enhancement of the phase separation by the shear in the very initial stages after TMS=0, as well as partial melting and breakage mechanism after the application of shear at TMS =10 000 (solution) and TMS=5000 (melt) (see discussion of Fig. 7), are strongly correlated with the removal and creation of interconnections that can be deduced from the Euler characteristic for the average density threshold choice, $h=\rho^0$ (Fig. 8, left). In particular, shear from the beginning leads to an enhanced removal of connections (see Fig. 8, top left, and inset in bottom left). We see that our interpretation, that partial melting prior to reformation of structures proceeds via first breakage of domains and then recombination of them in the flow direction, is not complete. A drop in the Euler number at the instance where shear was applied (△ in Fig. 8, left) manifests that the sequence can be reverse. First new interconnections are formed (in the direction of flow presumably) and only then unfavorable interconnections (in the way of flow) break. We conclude, without looking into 3D images that the final structure consists of perfect cylinders. We also see that the instance at which the shear is applied on the stronger separated system (melt) has no dramatic effect on the topological dynamics of the structure, which does not contradict, however, with the interpretations based on Fig. 7 (bottom). The Euler characteristics for higher density values ($h=0.5$) gives us addition information, Fig. 8 (right column). The behavior is very different for the solution and the melt. At the very beginning in a weakly separated system (solution) the high-density modes (○) form an interconnected network without shear. Later on this network breaks into micelles. On the contrary, in the presence of shear (Fig. 4, top, ○) the micelles are formed already in the very beginning. Therefore the shear suppresses interconnections in the initial stages of phase separation in solution for both choices of threshold value [notice, that the initial Euler numbers for $h=\rho^0$ (squares) are much lower without shear as well]. When shear is applied at TMS=10 000, the high-density values, $h=0.5$, show breakage of cylinders into spherical micelles, while in case of the average density threshold interconnections are formed (opposite bumps in graphs in Fig. 8, right top). Both structural changes lead to aligned cylinders at the end. Remarkably, breakage into micelles is not seen for the melt when shear is applied at TMS=5000 (Fig. 8, right bottom, ○). This suggests why the less segregated solution system has less defects at the end than the stronger segregated melt (see Fig. 2). The solution system has a rather flexible structure, on which shear, applied at a later instance, has a generic effect: it recombines the high-density micelles and breaks up the connections at the average density level that are not in the shear direction. The absence of the intermediate micellar phase (at least in noticeable quantity) for high densities in the melt makes it much more difficult to reorient in shear flow. The suppression of high-density micelles by shear in the melt is also seen in another striking difference in Euler number graphs for the two systems. The high-density modes of the melt system at the very first stages of phase separation in the absence of shear are spherical micelles (Fig. 8, right bottom, ○), contrary to interconnections in the solution. These micelles are absent if shear was applied from the very beginning (Fig. 4, bottom, ○), although it is possible that the structure is a collection of interconnections and some spheres, as the total Euler number is not very low. In the absence of shear, the micelles promptly form an interconnected network and the evolution follows the average density modes (Fig. 8, right bottom). This difference could be due to the compositional difference between diblock copolymer melt and triblock copolymer solution and is beyond of the scope of the present paper.

V. CONCLUSION

We have used Minkowski functionals for the determination of the kinetic pathways of the dynamics of block copolymer morphologies in an applied shear flow. As the application of Minkowski functionals requires binary valued pictures, a very important step is the thresholding procedure that is applied on the simulation data prior to the Minkowski functional calculation. The important question is: what threshold value or values contain redundant information? Using *a priori* knowledge of our system, we make a physically motivated choice for the two threshold values that we need for our analysis. We find that a minimal set of two threshold values (one from which should be equal to an average density value and another to a higher density value) is sufficient to unraffle the phase separation kinetics. This approach enhances the efficiency of the morphological analysis and minimizes the amount of data enormously.

We have used the Euler characteristics for the two choices of the threshold to extract the kinetic pathways for a diblock melt and triblock solution. Although the systems have different composition and different degree of segregation, both systems form cylinders in bulk; under shear these cylinders orient into a perfect hexagonal packing. In the absence of shear, quenching a homogeneous mixture leads to different phase separation kinetics for the two systems under consideration. In the high-density mode the melt separates into disconnected micelles, which merge into an interconnected network very fast. In the same mode the solution first forms an interconnected network and then partially disassembles into micelles. When shear is applied to the existing structures at a later instance it does not have a noticeable effect on the connectivity in the melt. For the solution, shear enhances the formation of disconnected micelles. However, in the average density mode the pathway of both system is qualitatively similar. The shear applied to the existing structures at a later instance increases connectivity in the first moments after application.

The effect of shear on the early stages of phase separation was also studied. We observe that, in the initial stages, shear enhances phase separation both in the melt and the solution. After the initial stages, there is a period of suppression of phase separation by shear due to the breakage of structures by shear. This period is very short for the solution as this system is weakly segregated and very flexible. A rea-

son for less flexibility in the stronger segregated melt is the suppression of the micellar phase by shear.

We conclude that lower phase segregation enhances the orientation kinetics under shear. Shear has a different influence on the initial and later stages of phase separation, which also depends on the degree of phase separation.

Finally, we point to the amazing similarity of the time dependent plots of the segregation parameter (Fig. 7) and the Euler characteristic (left column in Fig. 8) for both systems under consideration. These parameters are of completely different mathematical constructions, and we therefore cannot give an easy explanation for this fact. This observation will hopefully challenge others.

ACKNOWLEDGMENTS

The supercomputer resources were provided by a grant of NCF at the High-Performance Computing Facility (SARA) in Amsterdam. We thank Kristel Michielsen (University of Groningen, The Netherlands) for early calculations (that were not included in the present work) and Klaus Mecke (MPI Stuttgart, Germany) for stimulating discussions.

[1] G. J. A. Sevink, A. V. Zvelindovsky, and J. G. E. M. Fraaije, in *Mesoscale Phenomena in Fluid systems. ACS Symposium Series No. 861*, edited by F. Case and P. Alexandridis (ACS, Washington, DC, 2003), p. 258.
[2] G. Hadziioannou, A. Mathis, and A. Skoulios, Colloid Polym. Sci. **257**, 15 (1979).
[3] G. Schmidt, W. Richtering, P. Lindner, and P. Alexandridis, Macromolecules **31**, 2293 (1998).
[4] J. Raczkowska, J. Rysz, A. Budkowski, J. Lekki, M. Lekka, A. Bernasik, K. Kowalski, and P. Czuba, Macromolecules **36**, 2419 (2003).
[5] J. Becker, G. Grun, R. Seemann, H. Mantz, K. Jacobs, K. R. Mecke, and R. Blossey, Nat. Mater. **2**, 59 (2003).
[6] Y. Mao, T. C. B. McLeish, P. I. C. Teixeira, and D. J. Read, Eur. Phys. J. D **6**, 69 (2001).
[7] G. Kerch, Macromol. Symp. **158**, 103 (2000).
[8] K. Michielsen, H. de Raedt, and J. G. E. M. Fraaije, Prog. Theor. Phys. Suppl. **138**, 543 (2000).
[9] A. Aksimentiev, K. Moorthi, and R. Holyst, J. Chem. Phys. **112**, 6049 (2000).
[10] J. S. Gutmann, P. Muller-Buschbaum, and M. Stamm, Faraday Discuss. **112**, 285 (1999).
[11] M. Fialkowski, A. Aksimentiev, and R. Holyst, Phys. Rev. Lett. **86**, 240 (2001).
[12] K. R. Mecke and H. Wagner, J. Stat. Phys. **64**, 843 (1991).
[13] K. R. Mecke, J. Phys.: Condens. Matter **8**, 9663 (1996).
[14] K. R. Mecke, Fluid Phase Equilib. **150–151**, 591 (1998).
[15] K. R. Mecke, Int. J. Mod. Phys. B **12**, 861 (1998).
[16] K. R. Mecke, Phys. Rev. E **56**, R3761 (1996).
[17] A. L. Mellot, Phys. Rep. **193**, 1 (1990).
[18] K. R. Mecke, T. Buchert, and H. Wagner, Astron. Astrophys. **288**, 697 (1994).
[19] K. Michielsen and H. de Readt, Phys. Rep. **347**, 461 (2001).
[20] A. V. Zvelindovsky, G. J. A. Sevink, K. S. Lyakhova, and P. Altevogt, Macromol. Theory Simul. **13**, 140 (2004).
[21] J. G. E. M. Fraaije, J. Chem. Phys. **99**, 9202 (1993).
[22] B. A. C. van Vlimmeren, N. M. Maurits, A. V. Zvelindovsky, G. J. A. Sevink, and J. G. E. M. Fraaije, Macromolecules **32**, 646 (1999).
[23] F. Drolet and G. H. Fredrickson, Phys. Rev. Lett. **83**, 4317 (1999).
[24] G. H. Fredrickson, V. Ganesan, and F. Drolet, Macromolecules **35**, 16 (2002).
[25] M. Doi and D. Chen, J. Chem. Phys. **90**, 5271 (1989).
[26] T. Ohta, Y. Enomoto, J. L. Harden, and M. Doi, Macromolecules **26**, 4928 (1993).
[27] A. V. Zvelindovsky, G. J. A. Sevink, B. A. C. van Vlimmeren, N. M. Maurits, and J. G. E. M. Fraaije, Phys. Rev. E **57**, R4879 (1998).
[28] A. V. Zvelindovsky, G. J. A. Sevink, and J. G. E. M. Fraaije, Phys. Rev. E **62**, R3063 (2000).
[29] K. Michielsen and H. de Readt, Comput. Phys. Commun. **132**, 94 (2000).
[30] K. R. Mecke, (private communication).
[31] A. V. M. Zvelindovsky, B. A. C. van Vlimmeren, G. J. A. Sevink, N. M. Maurits, and J. G. E. M. Fraaije, J. Chem. Phys. **109**, 8751 (1998).